ACS OMEGA

Article

Cite This: ACS Omega 2019, 4, 18049−18060

http://pubs.acs.org/journal/acsodf

Disorder-to-Order Markers of a Cyclic Hexapeptide Inspired from the Binding Site of Fertilin β Involved in Fertilization Process

Belén Henández,[†,‡] Pauline Legrand,[§,∥] Sophie Dufay,[∥] Rabah Gahoual,[§] Santiago Sanchez-Cortes,[⊥] Sergei G. Kruglik,[#] Jean-Roch Fabreguettes,[∥] Jean-Philippe Wolf,[∇,○] Pascal Houzé,[§,◆] and Mahmoud Ghomi*[,†,‡]

[†]Laboratoire Matrice Extracellulaire et Dynamique Cellulaire (MEDyC), UMR 7369, Université de Reims, Faculté des Sciences, Moulin de la Housse, 51687 Reims Cedex 2, France

[‡]Sorbonne Paris Cité, Université Paris 13, Groupe de Biophysique Moléculaire, UFR Santé-Médecine-Biologie Humaine, 74 Rue Marcel Cachin, 93017 Bobigny Cedex, France

[§]Unité de Technologies Chimiques et Biologiques pour la Santé (UTCBS), CNRS UMR 8258-U1022, Faculté de Pharmacie Paris Descartes, Université Paris Descartes, 75006 Paris, France

[∥]Agence Générale des Equipements et Produits de Santé (AGEPS), Assistance Publique-Hôpitaux de Paris (AP-HP), 75005 Paris, France

[⊥]Instituto de Estructura de la Materia, IEM-CSIC, Serrano 121, 28006 Madrid, Spain

[#]Laboratoire Jean Perrin, Sorbonne Université, CNRS UMR 8237, 75005 Paris, France

[∇]Sorbonne Paris Cité, Université Paris Descartes, Faculté de Médecine, Assistance Publique-Hôpitaux de Paris (AP-HP), Hôpital Universitaire Paris Centre, Centre Hospitalier Universitaire (CHU) Cochin, Service d'Histologie-Embryologie-Biologie de la Reproduction, 75006 Paris, France

[○]Département Génomique, Epigénétique et Physiopathologie de la Reproduction, Institut Cochin, INSERM U1016, CNRS UMR8104, Université Paris Descartes, Sorbonne Paris Cité, 75006 Paris, France

[◆]Laboratoire de Biochimie, Hôpital Universitaire Necker-Enfants Malades, Assistance Publique-Hôpitaux de Paris (AP-HP), 75015 Paris, France

Supporting Information

ABSTRACT: Synthetic peptides mimicking the binding site of fertilin β to its receptor, integrin α6β1, were shown to inhibit sperm−egg fusion when added to in vitro media. In contrast, the synthetic cyclic hexapeptide, cyclo(Cys[1]-Ser[2]-Phe[3]-Glu[4]-Glu[5]-Cys[6]), named as cFEE, proved to stimulate gamete fusion. Owing to its biological specificity, this hexapeptide could help improve the in vitro fertilization pregnancy rate in human. In an attempt to establish the structure−activity relationship of cFEE, its structural dynamics was herein analyzed by means of ultraviolet circular dichroism (UV-CD) and Raman scattering. The low concentration CD profile in water, containing mainly a deep minimum at ∼202 nm, is consistent with a rather unordered chain. However, an ordering trend of the peptide loop has been observed in a less polar solvent such as methanol, where the UV-CD signal shape is formed by a double negative marker at ∼202/215 nm, indicating the presence of a type-II′ β-turn. Raman spectra recorded in aqueous samples upon a 100-fold concentration increase, still showed an important population (∼30%) of the disordered structure. The structural flexibility of the disulfide bridge was confirmed by the Raman markers arising from the Cys[1]-Cys[6] disulfide bond-stretch motions. Density functional theory calculations highlighted the formation of the type-II′ β-turn on the four central residues of cFEE (i.e., -Ser[2]-Phe[3]-Glu[4]-Glu[5]-) either with a left- or with a right-handed disulfide. The structure with a left-handed S−S bond, however, appears to be more stable.

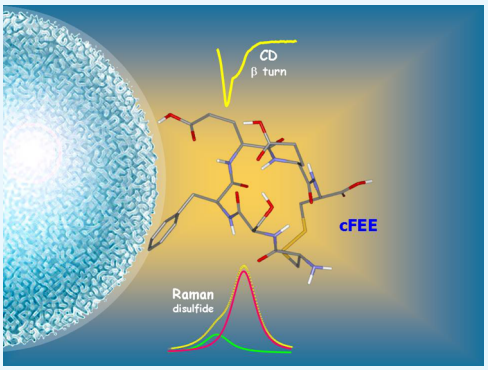

INTRODUCTION

fertilin β, also known as ADAM2, is part of a disintegrin and metalloprotease (ADAM) family of proteins. ADAMs are widely expressed with various functions in cell−cell and cell−matrix interaction. Their common feature is to express a

Received: June 24, 2019
Accepted: August 28, 2019
Published: October 22, 2019

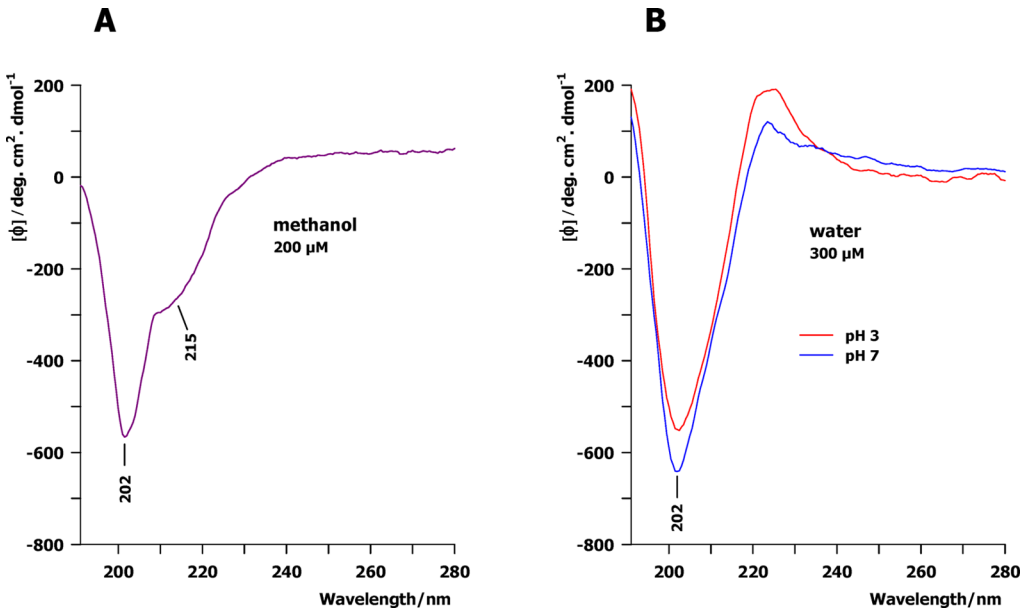

Figure 1. Room-temperature UV-CD spectra of cFEE displayed in the 190−280 nm region. (A) Data recorded in methanol at 200 μM. (B) Data recorded in aqueous samples at 300 μM as a function of pH.

disintegrin-like domain that could bind to receptors like integrins,[1] a family of heterodimeric transmembrane receptors composed of covalently linked and β subunits. Fertilin β is located on spermatozoa, whereas its binding receptor the integrin 6β1 is located on oocytes. Numerous studies have highlighted the importance of the binding between fertilin β and integrin 6β1 in the sperm−egg binding process, allowing their fusion.[2,3] Indeed, in vitro studies showed that sperm−egg fusion is greatly reduced when the interaction between fertilin β and integrin 6β1 is specifically inhibited. Such inhibition was performed by adding to in vitro media, synthetic peptides mimicking the binding site of the fertilin β (e.g., the disintegrin domain), so that they act as a competitor.[3−7] Therefore, the binding between fertilin β and integrin 6β1 was identified as a crucial step for egg−sperm fusion. However, attempts based on using gene knockout experiments have revealed that several sperm factors identified from the in vitro system are in fact not essential for in vivo fertilization.[8] Indeed, fertilization was proven to be still possible when genes of fertilin β are deleted.[9−11] Fertilin β is actually believed to play a role in sperm transport in the oviduct rather than in sperm−oocyte fusion.[8] Nevertheless, regardless of its activity concerning the in vivo fertilization process, it is clear that the inhibition of the fertilin β binding to α6β1 inhibits egg−sperm fusion in vitro, thus becoming crucial importance upon the consideration of the in vitro fertilzation (IVF) approach.

The binding sequence of fertilin β is species specific. In human, this sequence corresponds to -Phe-Glu-Glu- (or FEE).[12] Ziyyat et al.[13] evaluated the role of fertilin β in human gamete fusion, by using a peptide reproducing its binding site to integrin 6β1. As the binding domain of fertilin β is localized at the top of a hairpin loop, to reproduce its natural conformation, a cyclic hexapeptide, NH_2-CSFEEC-COOH (cyclic part underlined), hereafter referred to as cFEE, was used. Unexpectedly, while most peptides and recombinant forms of fertilin inhibit sperm−egg fusion, cFEE was shown to lead to an increase of the gamete fusion.[13] In fact, cFEE was shown to bind to the oocyte membrane, simulating spermatozoon contact by inducing the displacement of the adhesion protein to the oocyte surface. Similar results were observed upon a clinical trial on mice by the use of the mouse sequence equivalent to cFEE (cQDE), leading to the improved IVF pregnancy rate in mice.[14] It has been thought that this specific biological effect of cFEE in vitro might be explained by both its amino acid composition and cyclic structure maintained by a disulfide bridge between its two terminal cysteines.[13,14] Nevertheless, a convincing explanation has not yet been provided.

Therefore, it appeared to us interesting to analyze the structural dynamics of this cyclic hexapeptide to help understand its specific action (vide supra) that can be envisaged in IVF pregnancy rate improvement in human. On the other hand, the knowledge of the conformational features of cFEE might lead to design other peptides with higher IVF success rates. Herein, at a first stage of these investigations, the structural analysis of cFEE has been undertaken by means of optical spectroscopic techniques such as circular dichroism (CD) and Raman scattering. During the past decade, the joint use of these approaches has rendered possible the analysis of the structural properties of both linear and cyclic peptides in aqueous media as a function of their length, concentration, as well as of the ionic strength, pH, and time.[15−21] Furthermore, in many cases, the role of the surrounding solvent, in going from high to low dielectric media, favoring the intermolecular interactions rather than those from the intramolecular type has also been elucidated.[15−18] As concerns about the cyclic peptides, while CD spectra give rapid and general information on their folding type, Raman spectra provide details on the rate of different secondary structural elements (disordered, turn, and strand) appearing in their closed part.[19−22]

RESULTS AND DISCUSSION

LC-MS/MS Analysis. The characterization based on reverse phase liquid chromatography hyphenated to high-resolution tandem mass spectrometry (LC-MS/MS) was made with the aim of providing orthogonal information regarding the integrity of the cyclic peptide and to eventually identify the presence of interfering impurities. Considering the obtained

DOI: 10.1021/acsomega.9b01885
ACS Omega 2019, 4, 18049−18060

chromatogram, the presence of the hexapeptide cFEE was confirmed. $[M + H]^+$ was observed at 715.2051 (Figure S1A, Supporting Information), with a mass deviation from the theoretical value not exceeding 2.5 ppm. This represents conventionally the instrumental performance. The present data with previous ones[24] and the resolution provided by the MS instrument allowed elucidating the isotopic distribution of cFEE, being in complete correlation with its cyclic structure.

Concomitantly, during the analysis, fragmentation by collision-induced dissociation (CID) was performed to investigate more precisely the structure of the compound. As illustrated in Figure S1B (Supporting Information), MS/MS spectra corresponding to cFEE mainly demonstrated the detection of the fragments corresponding to the b-ion series. The identified fragments demonstrated to be particularly consistent with the amino acid sequence of the cFEE peptide. Except cFEE, the investigation of LC-MS/MS data did not reveal the presence of any additional compound, thus excluding the presence of probable impurities.

UV-CD Markers. UV-CD spectra recorded at 300 μM in methanol and water are displayed in traces A and B of Figure 1, respectively. Upon comparison, the effect of the solvent type on the observed spectra can be clearly seen on CD spectra. In both media, all the spectra are mainly characterized by a deep minimum at ∼202 nm. However, in methanol (Figure 1A), a distinct shoulder at ∼215 nm was detected at the long wavelength side of the main minimum. On the contrary, the pH effect (from acidic toward neutral pH, Figure 1B) is reflected by an overall decrease of the negative band at ∼202 nm, as well as an increase of the positive signal at ∼220 nm, without changing the overall dichroic shape of the CD spectra. It can be reminded that the pK_a corresponding to the Glu side-chain protonation/deprotonation is ∼4.1. As a result, the two selected pH values favor as major population either the protonated (pH 3) or the deprotonated (pH 7) side chains of Glu^4 and Glu^5 residues.

The influence of the solvent polarity on the peptide structural features has been detailed previously.[15,16] Some linear peptides were reported to undergo a β-strand → α-helix transition from water (a polar solvent) to another having a lower dielectric constant (alcohols). This effect has been interpreted by the capacity of a polar solvent to reinforce the intermolecular H-bonds, rather than the intramolecular ones.[15] Beyond the solvent polarity, the influence of peptide length, concentration, and eventually its exposure time to the solvent appeared to act as the key structuring elements.[16−18] In cyclic peptides, the closure constraint (imposed for instance by a disulfide bond), the length, and the amino acid composition of its closed part were shown to be the key elements in their structural behaviors.[19−21]

Focusing on UV-CD structural markers, a random chain is routinely characterized by a deep negative dichroic band at ∼198 nm,[25,26] whereas a loosely structured loop (i.e., subjected to a rapid interconversion of several instable turns) provides a slightly red-shifted negative CD signal to ∼202 nm.[19] As a consequence, the characteristic CD fingerprint of cFEE in water, independently of the pH value (Figure 1B), is consistent with the formation of an unordered/weakly ordered turn, whereas the double negative band shape reveals the presence of a structured loop formed in methanol (Figure 1A). Previously, upon an extensive study of the CD and NMR data obtained from 10 gramicidin S cyclic peptides, all adopting a reverse type-II′ β-turn, it has been highlighted that their CD profile is composed of a double negative bands at ∼202 and ∼215 nm. Furthermore, the dichroic ratio $[\Phi_2]/[\Phi_1]$, where $[\Phi_2]$ and $[\Phi_1]$ are the normalized ellipticities corresponding to the higher (∼215 nm) and lower (∼202 nm) wavelength components of the characteristic double negative CD fingerprint, respectively, can be taken as an indicator of their β-turn stability.[27] More precisely, while a compact (or highly stable) type-II′ β-turn gives a $[\Phi_2]/[\Phi_1]$ ratio close to unity,[21] a less stable turn of the same family provides a lower (<1) ratio. Following these evidences, the CD band shape of cFEE (Figure 1A), with a $[\Phi_2]/[\Phi_1]$ ratio of ∼0.4, is consistent with a rather instable (mobile) type-II′ β-turn in methanol. Other types of β-turns provide, noteworthy, a CD signal different from those observed in cFEE. For instance, a type-I β-turn is characterized by double minima at ∼208/222 nm, resembling that traditionally assigned to an α-helix, a type-II β-turn gives a positive band located within the 190−210 nm region, and finally, a reverse type-I′ β-turn provides a broad negative band at ∼215 nm.[25]

Raman Markers. Raman spectra of cFEE, recorded at 30 mM in the middle wavenumber region in aqueous samples, are displayed in traces A and B of Figure 2 corresponding to pH 3

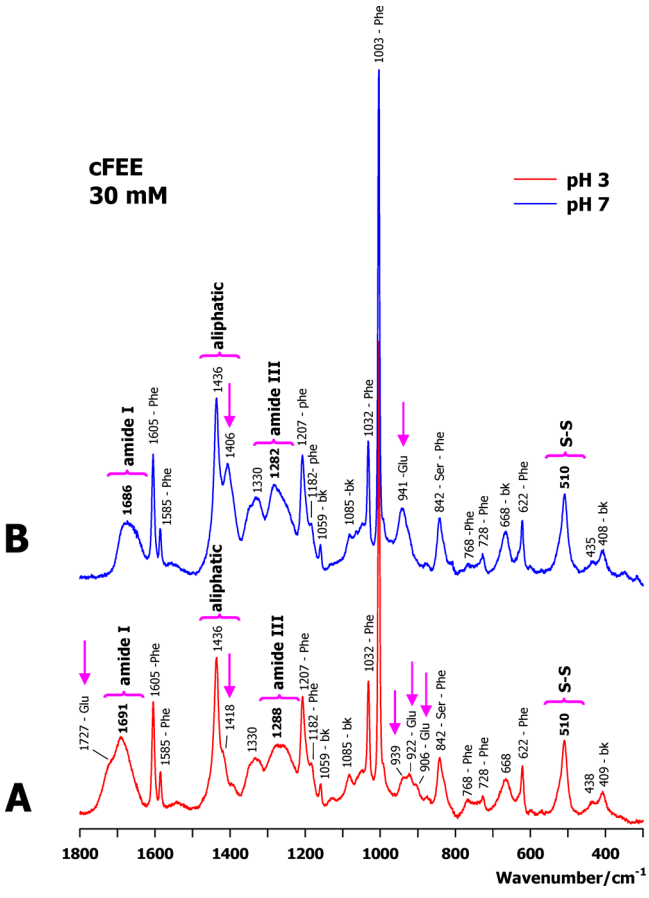

Figure 2. Room-temperature Raman spectra recorded from the aqueous samples of cFEE. The spectra obtained at (A) pH 3 and (B) pH 7. The tentative assignment of the main Raman bands is made on the basis of the data corresponding to free AAs (Figure 3). Amide (I and III) and disulfide bond regions are noted. See Figures 4 and 5 for band decomposition of these particular regions. The characteristic Raman bands sensitive to the Glu side-chain protonation/deprotonation are marked by pink arrows. Phe and bk designate the Raman bands assigned to phenylalanine residue and backbone, respectively.

DOI: 10.1021/acsomega.9b01885
ACS Omega 2019, 4, 18049−18060

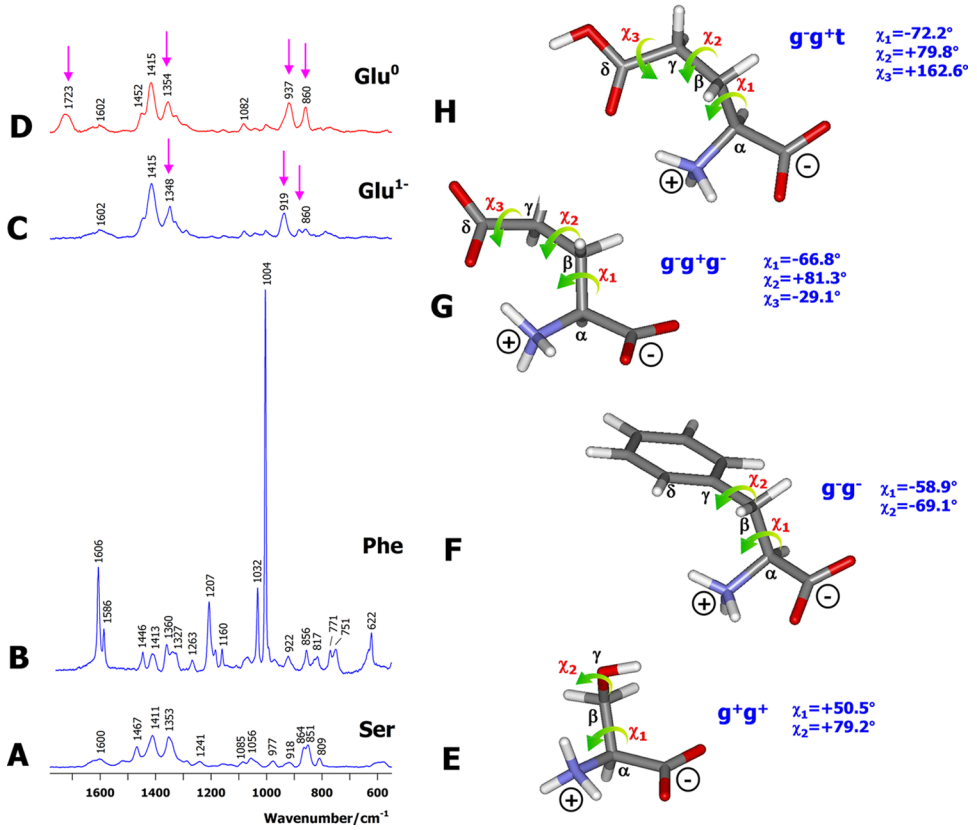

Figure 3. Room-temperature Raman spectra obtained from the aqueous samples of free AAs together with their lowest energy zwitterionic species. Raman spectra of (A) Ser, (B) Phe, (C) Glu^{1-} (Glu with a deprotonated side chain), and (D) Glu^{0} (Glu with a protonated side chain). The characteristic Raman bands sensitive to the Glu side-chain protonaton/deprotonation are marked by pink arrows in (C) and (D). Lowest energy conformers of (E) Ser, (F) Phe, (G) Glu^{1-}, and (H) Glu^{0}. Side-chain torsion angles values and global orientations are reported at the right side of the graphical representations (E–H). See text for details. Theoretical level: DFT/B3LYP/6-311++G(d,p).

and 7, respectively. To achieve a reliable assignment of the observed Raman bands, we resorted to those from their building blocks. For this, the Raman spectra of free Ser, Phe, and Glu are shown in Figure 3A–D. Because of their full analysis in both solid and solution samples,[28] the Raman data of cysteine (i.e., Cys-Cys dimer with a disulfide bond) were not reported here. Selected pH values of the solution samples of free AAs favored their zwitterionic species (with NH_3^+/COO^- backbone end groups). This fact can be verified for instance by the broad band at ∼1602 cm^{-1} corresponding to the carboxylate (COO^-) asymmetric stretching mode (Figure 3A,C,D). Because of the absence of any internal reference, to facilitate their comparison, all spectra were normalized to their intensities in the 1500–1400 cm^{-1} region, arising from the aliphatic modes (angular bending motions of CH_2 groups). The strongest Raman bands naturally correspond to the Phe aromatic markers located at 1606, 1586, 1207, 1032, 1004, and 622 cm^{-1} (Figure 3B). It is interesting to note that the spectrum of Glu^0 species (with a protonated side chain) recorded at an acidic pH (2.9) clearly reveals the presence of the broad band at ∼1723 cm^{-1} assignable to the carbonyl (C═O) bond-stretch marker resulting from the side-chain head group (COOH) (Figure 3D). At pH 6, upon the predominance of Glu^{1-} species in the solution (with a deprotonated side-chain head group COO^-), the carbonyl marker expectedly vanishes (Figure 3C). The comparison between the spectra of Glu^0 and Glu^{1-} species permits locating the markers affected by the side-chain protonation/deprotonation within three distinct regions, that is, 1730–1700, 1350–1300, and 950–850 cm^{-1} (bands marked by pink arrows in Figure 3C,D). For the detailed assignment of the Raman bands, see refs 29 and 30 for Phe and ref 31 for Ser. As far as Glu is concerned, we present in Table S1 (Supporting Information) the theoretical wavenumbers of the main Raman bands along with their assignments from the presently performed DFT calculations on the lowest energy conformers of both Glu^{1-} and Glu^0 species (Figure 3G,H) (see also Results and Discussion for details). In particular, the Raman markers shown by pink arrows in Figure 3C,D are assigned to a mixture of side-chain/backbone vibrational motions, thus explaining their sensitivity to the side-chain head group COOH → COO^- conversion.

The Raman bands observed in free AAs allowed us to propose in Figure 2A,B the tentative assignment of cFEE spectra. Whatever pH, the Raman intensity is expectedly dominated by that arising from Phe[3]. Nevertheless, the relative intensity of Glu markers is strong enough to permit appreciation of the changes occurring upon side-chain protonation/deprotonation (see medium bands marked by pink arrows in Figure 2A,B). For instance, the appearance of a shoulder at ∼1727 cm^{-1} at pH 3 should be noticed (Figure 2A), vanishing at pH 7 (Figure 2B). In the 950–900 cm^{-1} region, the broad and dissymmetric band peaking at ∼941 cm^{-1} at pH 7 (Figure 2B) is transformed to a set of partially resolved bands at ∼933, 922, and 906 cm^{-1} at pH 3 (Figure 2A).

DOI: 10.1021/acsomega.9b01885
ACS Omega 2019, 4, 18049–18060

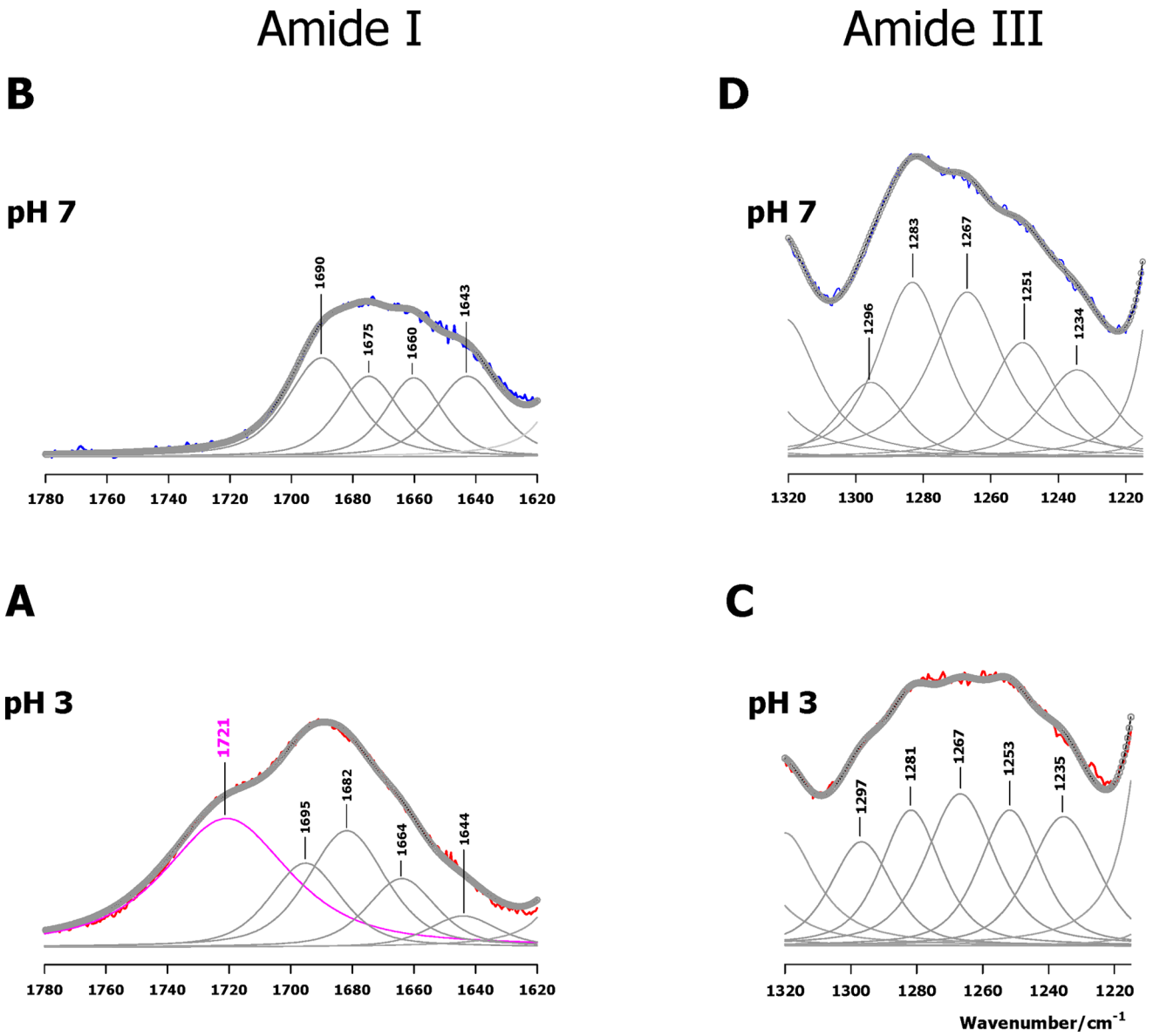

Figure 4. Band decomposition in the amide regions of Raman spectra. (A, B) Amide I and (C, D) amide III are decomposed at pH 7 (top) and pH 3 (bottom). Observed spectra are in red (pH 3) and blue (pH 7) colors. Band components are drawn in gray. Empty circles correspond to the sum of the components. See text for details and Table 1 for normalized contributions and their assignments to different secondary structural elements (random, β-strand, and turn). Note that the component at 1721 cm^{-1} (pink color in (A)) arises from the stretching mode of the carbonyl bond appearing upon the Glu side-chain protonation at pH 3.

The comparison between the Raman spectra of cFEE (Figure 2A,B) and those from free AAs (Figure 3A−D) also allows analyzing the vibrations arising from the peptide backbone, referred to as amide I (1750−1625 cm^{-1}) and amide III (1320−1225 cm^{-1}) modes. Both amide regions involve broad and barely resolved bands, consistent with the presence of several secondary structural elements in cFEE. Band decomposition in amide (I and III) regions (Figure 4) leads us to achieve detailed structural information. The protocol used for band decomposition was established on the basis of the previous works on linear[16−18] and cyclic[19−22] peptides. Table 1 shows the normalized contributions (as expressed in percent) of the band components at pH 3 (Figure 4A,C) and pH 7 (Figure 4B,D). Comparable results were obtained from amide (I and III) regions, confirming the reliability of band decomposition and corresponding assignments. As far as the influence of pH is concerned, apart from a slight decrease of ordered elements (turn and β-strand) versus a slight increase of random chain contribution, no other perceptible effect can be noticed in going from an acidic toward a neutral pH value (Table 1).

The 550−480 cm^{-1} region of the Raman spectra involving the S−S bond stretching vibrations is zoomed in Figure 5. Independently of the pH value, band decomposition makes clearly appear two components at ∼509 and ∼525 cm^{-1}, assignable to two different types of rotamers around the S−S linkage in cFEE (see for details ref 28); the normalized area corresponding to these two components is estimated as ∼80% (for the ∼509 cm^{-1} component) versus ∼20% (for the ∼525 cm^{-1} component). Although the rotamer relative to the ∼509 cm^{-1} component should correspond to the major disulfide rotamer in aqueous solution, the presence of the second

DOI: 10.1021/acsomega.9b01885
ACS Omega 2019, 4, 18049−18060

Table 1. Normalized Contributions of Different Secondary Structural Elements As Determined by the Analysis of Amide (I and III) Regions[a]

amide I (components)	turn (%)	β-strand (%)	random (%)
pH 3			
1695			27
1682	41		
1664		22	
1644	10		
pH 7			
1690			32
1675	24		
1660		20	
1643	24		
amide III (components)	**turn (%)**	**β-strand (%)**	**random (%)**
pH 3			
1297	15		
1281	19		
1267			25
1253	20		
1235		21	
pH 7			
1296	11		
1283	28		
1267			30
1250	17		
1234		14	
total	**turn (%)**	**β-strand (%)**	**random (%)**
amide I (pH 3)	51	22	27
amide III (pH 3)	54	21	25
amide I (pH 7)	48	20	32
amide III (pH 7)	56	14	30
accuracy ±5%			

[a]The components are referred to by their maximum wavenumber expressed in cm^{-1}. See Figure 4 for band decomposition of amide (I and III) regions.

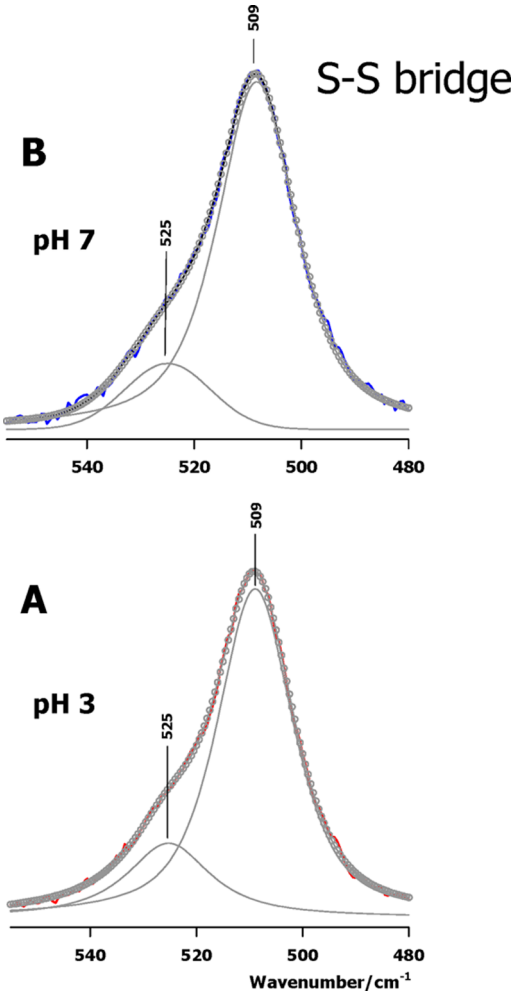

Figure 5. Band decomposition in the disulfide bond-stretch region of Raman spectra. Observed spectra are in (A) red (pH 3) and (B) blue (pH 7) colors. Band components are drawn in gray color. Empty circles correspond to the sum of components. See text for details.

component at ∼525 cm^{-1} with lower intensity reveals the conformational flexibility of the S−S linkage.

Type-II′ β-Turn Structural Models for cFEE. UV-CD spectra led us to presume that a loosely structured type-II′ β-turn can be formed in methanol (see above UV-CD Markers for details). It is worth emphasizing that there exist two reverse type β-turns, referred to as type-I′ and type-II′. Both of them are considered as frequently occurring β-turns in proteins.[36,37] Briefly, a β-turn is composed of four residues, generally numbered as i, $i + 1$, $i + 2$, and $i + 3$ in which the chain direction change is made possible by the special values of the backbone torsion angles (φ, ψ) assigned to the two middle $i + 1$ and $i + 2$ residues.[32,33] Particularly, in a type-II′ β-turn, the mentioned angles fluctuate around the following mean values ($\varphi_{i+1} \sim +60°$, $\psi_{i+1} \sim -120°$, $\varphi_{i+2} \sim -80°$, $\psi_{i+2} \sim 0°$).

To prepare the initial conformers of cFEE, we took an advantage of the extensive structural data corresponding to a synthetic cyclic octapeptide, named octreotide (or Sandostatin). Octreotide with the primary sequence N^{ter}-D-Phe[1]-cyclo(Cys[2]-Phe[3]-D-Trp[4]-Lys[5]-Thr[6]-Cys[7])-Thr(ol)[8] is one of the rare therapeutic peptides for which crystal,[34] NMR,[35] CD, and Raman[20,22] data, as well as DFT calculations,[36] are available. All these data confirm a type-II′ β-turn formed on the four central residues (-Phe[3]-D-Trp[4]-Lys[5]-Thr[6]-) of this peptide. Supposing that a similar turn can also be formed on the four central residues of cFEE (-Ser[2]-Phe[3]-Glu[4]-Glu[5]-), the backbone torsion angles (φ, ψ, ω) of octreotide[36] were transferred to the initial structure of cFEE. As far as the torsion angles defining the orientation of the side chains of Ser[2], Phe[3], Glu[4], and Glu[5] are concerned, we resorted to the DFT data existing on free AAs reported either in the previous investigations on Phe[37] and Ser[31] or derived from the presently performed calculations on Glu. The lowest energy conformers of Ser, Phe, Glu^0, and Glu^{1-} are displayed in Figure 3E−H, respectively. At the right side of each conformer, the values of their side-chain torsion angles, that is, (χ_1, χ_2) for Ser and Phe and (χ_1, χ_2, χ_3) for Glu. As far as the cysteine (Cys[1]-Cys[6]) conformation is concerned, we were inspired from a systematic structural analysis on the functional disulfide bridges in proteins.[38−41] The conclusion of this study was that a set of five torsion angles (χ_1, χ_2, χ_3, χ_2', χ_1') defined around the five chemical bonds (−Cα−Cβ−S−S−Cβ′−Cα′−) along the cysteine moiety are necessary to accurately define the conformational feature of a given S−S bridge. The torsion angles involved in the optimized structure of octreotide were ($\chi_1 = -166°$, $\chi_2 = +73°$, $\chi_3 = -97°$, $\chi_2' = +111°$, $\chi_1' = -179°$).[36] It is to be noted that this set of torsion angles corresponds to a left-handed S−S bridge because of the negative sign assigned to the χ_3 angle defined around the S−S

DOI: 10.1021/acsomega.9b01885
ACS Omega 2019, 4, 18049−18060

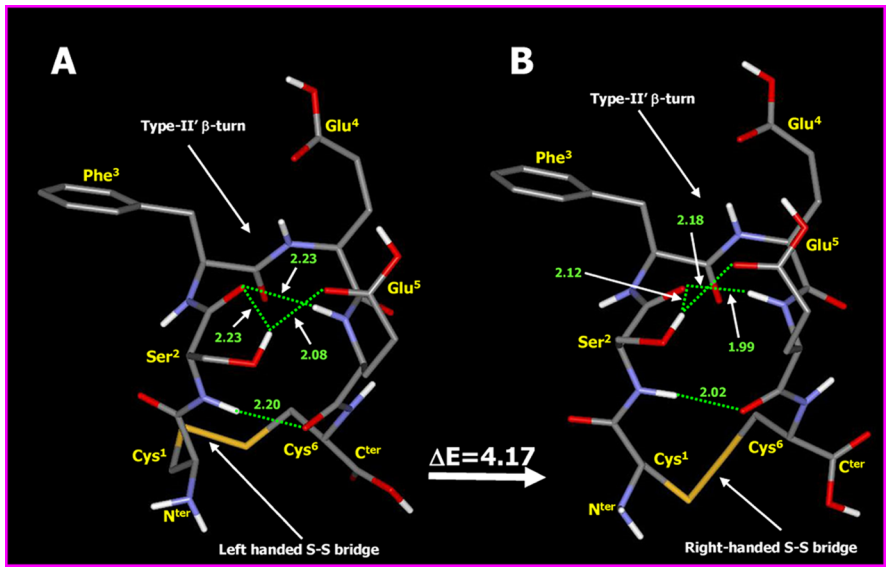

Figure 6. Graphical representation of the optimized structures of cFEE in a polarizable continuum mimicking methanol. The structures having (A) a left-handed and (B) a right-handed disulfide bridge. The locations of the type-II′ β-turn and disulfide bridge are noted. Intramolecular H-bonds are drawn in green broken lines, and their lengths (in Å) are reported. The energy difference between the two structures (ΔE in kcal/mol) is mentioned. Theoretical level: DFT/B3LYP/6-31G(d).

Table 2. Backbone and Side Chain Torsion Angles of cFEE Structures As Determined by DFT calculations[a]

Structure with a left-handed disulfide linkage (L)							Structure with a right-handed disulfide linkage (R)						
Residue	Backbone angles	Values	Conformation	Side chain angles	Values	Conformation	Residue	Backbone	Values	Conformation	Side chain	Values	Conformation
Cys^1	φ	-----		*			Cys^1	φ	-----		*		
	ψ	+70.1		*				ψ	+128.3		*		
	ω	-176.9		*				ω	+173.3		*		
Ser^2	φ	-88.3	↑	χ_1	+57.9		Ser^2	φ	-121.1	↑	χ_1	+58.1	
	ψ	+70.5		χ_2	+72.3	g^+g^+		ψ	+90.0		χ_2	+66.3	g^+g^+
	ω	-176.2						ω	+179.7				
Phe^3	φ	+60.7		χ_1	-63.3		Phe^3	φ	+54.3		χ_1	-61.2	
	ψ	-102.9		χ_2	-80.0	g^-g^-		ψ	-120.2		χ_2	-80.0	g^-g^-
	ω	-177.7						ω	-177.2				
Glu^4	φ	-65.4		χ_1	-61.7		Glu^4	φ	-62.4		χ_1	-62.9	
	ψ	-35.2		χ_2	+87.3			ψ	-28.1		χ_2	+86.3	
	ω	-178.9		χ_3	+170.9	g^-g^+t		ω	+179.3		χ_3	-167.0	g^-g^+t
Glu^5	φ	-84.5		χ_1	-59.2		Glu^5	φ	-82.1		χ_1	-59.0	
	ψ	+79.0		χ_2	+82.6			ψ	+83.1		χ_2	+84.3	
	ω	-172.0		χ_3	-149.5	g^-g^+t		ω	-172.9		χ_3	-139.6	g^-g^+t
Cys^2	φ	-133.0		*			Cys^2	φ	-154.0		*		
	ψ	+44.5		*				ψ	-37.0		*		
	ω	-----		*				ω	-----		*		

Type-II′ β-turn

[a]DFT calculation at the B3LYP/6-31G(d) level on the hexapeptide embedded in a polarizable continuum mimicking methanol. For the graphical representations, see Figure 6. Torsion angles are expressed in degrees. φ, ψ, and ω refer to the backbone torsion angles of the residues involved in the structure of the hexapeptide.χ_1, χ_2, and χ_3 torsion angles allow the orientation of the side chain of a given residue to be determined. Asterisk (*) corresponds to side-chain torsion angles of the cysteine (Cys^1-Cys^6) moiety that are reported in Figure 7 along with the corresponding graphical representation of the disulfide bridge.

bond. To analyze the effect of the S−S bridge handedness, we have also constructed a second initial conformer having a right-handed S−S linkage (having a positive χ_3 angle).

The optimized geometries of cFEE having either a left-handed (L) or a right-handed (R) disulfide linkage are reported in Figure 6A,B, respectively. Note that in both structures, Glu^4 and Glu^5 have a protonated side chain, reflecting a low dielectric constant environment such as methanol. For the same reason, the peptide backbone end groups were supposed to be neutral (NH_2/COOH). The optimized torsion angles of these conformers are reported in Table 2. As it can be seen, the type-II′ β-turn can be stabilized both with a left- or a right-handed disulfide. Nonetheless, a higher stability (with a lower relative energy) was predicted for the (L) structure (Figure 6). The interactions that stabilize both (L) and (R) structures are to be noticed as follows: (i) a quite short contact in the peptide backbone, (Ser^2)N−H···O−C(Glu^5), with a length varying between 2.02 and 2.20 Å, acting as the β-turn closing the H-bond and (ii) a set of three other H-bonds involving the side-chain head groups of Ser^2 (O−H), Glu^5 (COOH), as well as the backbone carbonyl C═O (Ser^2) and N−H (Glu^5) groups (with the lengths varying between 1.99 and 2.23 Å). To better appreciate the (L) and (R) rotamers of the S−S bridge, the cysteine moiety (Cys^1-Cys^6) is zoomed in Figure 7, along with the values of their characteristic torsion angles (χ_1, χ_2, χ_3, χ_2', χ_1'). Following

DOI: 10.1021/acsomega.9b01885
ACS Omega 2019, 4, 18049−18060

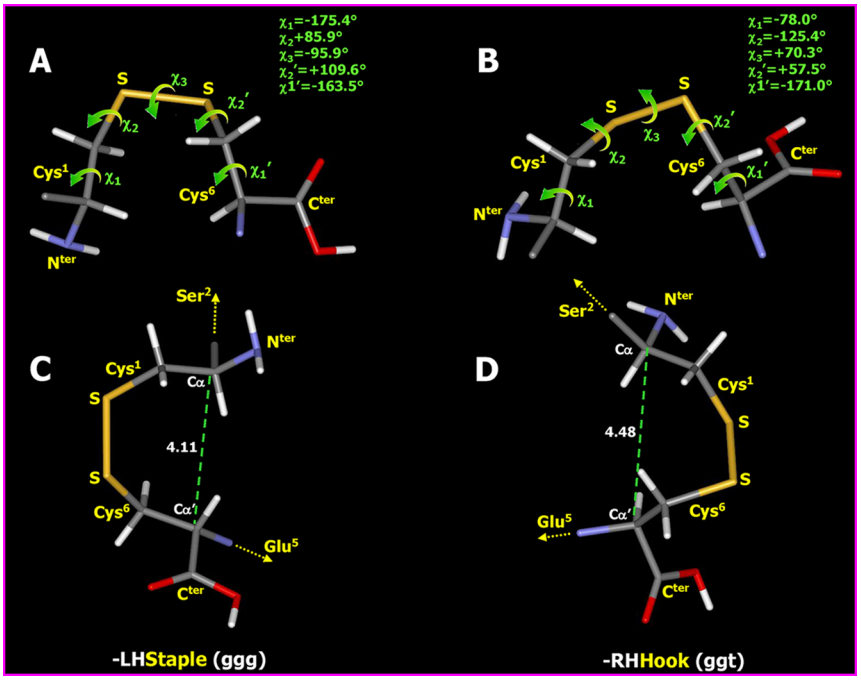

Figure 7. Zoom on the disulfide linkage of the optimized conformers of cFEE. Two views of each structure are reported. (A, C) left-handed disulfide bridge and (B, D) right-handed disulfide bridge. The distance between the Cα atoms belonging to Cys[1] and Cys[6] residues is reported in green broken lines of which the length (in Å) is also mentioned. The values of the five torsion angles defining the conformation of each disulfide bridge are mentioned at the right side of the representations (A) and (C). See text for details.

the original terminology initiated by Hogg and co-workers,[38] the optimized left-handed disulfide bridge can be considered as a "-LHStaple"-type rotamer (Figure 7C), whereas the right-handed one is rather a "-RHHook"-type rotamer (Figure 7D). In these notations, "LH" and "RH" designate left-handed and right-handed disulfides, respectively. "Staple" and "Hook" refer to their spatial shapes, and finally, the sign "-" reflects the negative values assigned to the terminal χ_1 and χ_1' torsion angles. It is worth noting that there also exists a traditional type of notation for defining the S−S bridge conformation, based on the g (gauche) and t (trans) orientations of the three middle torsion angles (χ_2, χ_3, χ_2'), without mentioning their signs. Following these notations, the left-handed S−S bridge corresponds to a "ggg" conformer, whereas the right-handed one can be classified as a "ggt" conformer. For further use of the optimized structures, the corresponding atomic Cartesian coordinates are reported in Table S2.

Comparison with Other Cyclic Peptides. To better understand the structural behavior of cFEE, we briefly compare it to that of other short cyclic peptides having preferentially an identical loop size. The natural hormone oxytocin, N^{ter}-cyclo(Cys[1]-Tyr[2]-Ile[3]-Gln[4]-Asn[5]-Cys[6])-Pro[7]-Leu[8]-Gly[9]-$CONH_2$, was provided in TFE (ε_r = 8.55),[42] a UV-CD profile similar to that obtained from cFEE in methanol (Figure 1A). In water (pH 7.3), its CD signal was rather consistent with an unordered chain.[43] Another structurally similar hormone, Arg-vasopressin, N^{ter}-cyclo(Cys[1]-Tyr[2]-Phe[3]-Gln[4]-Asn[5]-Cys[6])-Pro[7]-Arg[8]-Gly[9]-$CONH_2$, was shown to be unstructured in an aqueous environment (pH 6.9) as characterized by a deep negative CD profile peaking below 200 nm.[44] In other words, both mentioned neuropeptides presented a structural dynamics close to that of cFEE. Taking into account the fact that all three peptides possess a loop formed by six residues, their common structural features should undoubtedly arise from their amino acid composition and especially from those of the four loop residues, that is, -Tyr[2]-Ile[3]-Gln[4]-Asn[5]- (in oxytocin), -Tyr[2]-Phe[3]-Gln[4]-Asn[5]- (in Arg-vasopressin), and -Ser[2]-Phe[3]-Glu[4]-Glu[5]- (in cFEE). It is worth noting that all three sequences contain at least three residues with a pronounced hydrophilic character (selected among Ser, Tyr, Asn, Gln, and Glu residues). Recent DFT calculations highlighted the propensity of Phe and Tyr residues to be hydrated through the stabilization of short contacts between water hydrogen atoms and aromatic π-electron systems.[37] Nevertheless, the main structural difference between cFEE and the two mentioned neuropeptides seems to be in the handedness of their S−S bonds. In fact, previous Raman optical activity (ROA) measurements led to the conclusion that oxytocin and Arg-vasopressin contain both a right-handed S−S bond,[45] whereas the presently reported DFT calculations in methanol are consistent with a left-handed S−S bond as the major rotamer of cFEE (see above for details).

Structural Argument Put Forward for Explaining the Particular Biological Activity of cFEE. As the culture media for IVF is an aqueous media with a pH at 7.3, the reason behind the particular biological behavior of cFEE (see Introduction for details) might be dependent on its unordered character. To support this hypothesis on the structure−activity relationship of therapeutic peptides, we can mention the example of the natural hormone somatostatin-14 (SST-14), acting particularly as an inhibitor of the growth hormone secretion through its binding to one of the five G-protein-coupled receptors, referred to as SSTRi (i = 1,...,5).[46] SST-14 is a cyclic tetradecapeptide with a large size loop formed by 12 residues. This hormone was shown to form an unordered chain, as confirmed by CD, Raman,[19,21,22] and NMR data.[47−49] Apart from its loop size, the conformational flexibility of SST-14 can be related to the presence of seven intraloop

DOI: 10.1021/acsomega.9b01885
ACS Omega 2019, 4, 18049−18060

hydrophilic residues. Because of the plasma short half-life of SST-14, during the past decades, a series of synthetic analogues were elaborated and used in various somatostatin-based clinical therapies.[50,51] Among them, one can notice two widely spread cyclic octapeptides, octreotide and lanreotide, both forming a stable type-II′ β-turn on their four central residues.[20,21] Interestingly, these two analogues have shown a selective binding affinity toward two SST-14 receptors, that is, SSTR2 and SSTR5. The difference between the activities of SST-14 and its synthetic analogues might be better understood by their structural features. More explicitly, while SST-14 with its loose turn can equivalently interact with its five receptors presumably through an induced fit process,[52] the conformational restriction leads to considerably modulate its analogue activity.

CONCLUDING REMARKS

Because of the rapidity in acquisition and post-treatment of their data, the joint use of UV-CD and Raman spectra is now considered as a powerful method to probe the solution structural dynamics of the peptides, especially when they are unordered or barely structured. Herein, the application of this methodology evidenced that the cyclic therapeutic peptide cFEE adopts a rather unordered loop in aqueous media, without a perceptible structural transition from an acidic to a neutral pH value, being responsible for the side-chain protonation/deprotonation of its two adjacent Glu residues. Furthermore, Raman markers analyzed upon a ∼100-fold concentration increase still revealed that an important population of the random chain persists in cFEE. Nevertheless, a structural ordering trend has been observed in methanol through the appearance of type-II′ β-turn UV-CD markers. DFT calculations confirmed the formation of this reverse type β-turn in a molecular model embedded in a polarizable continuum mimicking methanol. It appeared that an intraloop H-bond network might contribute to maintain the structured loop in a low dielectric constant medium. It has thus been concluded that the disordered character of cFEE in water originates presumably from the preponderance of intermolecular H-bonds between the three hydrophilic residues (Ser^2, Glu^4, and Glu^5) with surrounding water molecules. Beyond the static QM calculations described in the present analysis, further molecular dynamics simulations in the presence of explicit water molecules would be necessary to highlight (i) the loop conformational flexibility within a sufficiently extended timescale and (ii) the residence time of water molecules on the loop residues. The latter point would lead us to a better understanding of the loop structural invariability either with protonated or with deprotonated Glu residues, probably caused by the solvent screening of their electrostatic interactions.

MATERIAL AND METHODS

Sample Preparation. The lyophilized sample of the cyclic peptide cFEE (Scheme 1, Supplementary Information) was purchased from Synprosis SA Laboratory (Fuveau, France). Solution samples were prepared by dissolving the hexapeptide in water taken from a Millipore filtration system (Merck, Molsheim, France). Stock solution of the hexapeptide was prepared at 30 mM, that is, ∼21.5 mg/mL. These samples were used in Raman spectroscopic measurements. Further dilution to lower concentrations was made for other experiments. Upon dissolution, the pH value of the peptide sample was ∼3; it was adjusted at higher values by adding NaOH (1 N) to aqueous samples. Free amino acids (AAs), Ser, Phe, and Glu, were purchased from Sigma-Aldrich (Saint-Quentin-Fallavier, France). The concentration of their aqueous samples used for Raman spectroscopy was 50 mM. The pH of Glu samples was adjusted to render possible the analysis of the side-chain protonation/deprotonation by Raman markers. Other used chemicals were also provided by Sigma-Aldrich.

Liquid Chromatography-Tandem Mass Spectrometry Analysis (LC-MS/MS). The hexapeptide was characterized by high-resolution mass spectrometry hyphenated to reverse phase liquid chromatography (RPLC) on a Waters BEH C18 (1.7 μm, 2.1 mm × 150 mm) column using an ultrahigh-performance liquid chromatography system (Waters ACQUITY UPLC; ACQUITY column manager-type ACQCM 1.40, binary solvent manager-type ACQ-BSM 1.65, sample manager-type ACQ-SM 1.65; Manchester, U.K.). The mobile phases were composed of 0.1% formic acid (FA) in water (mobile phase A) and 0.1% FA in acetonitrile (mobile phase B). The LC-MS/MS analysis was performed using a mobile phase flowrate of 100 μL/min and a column temperature of 40 °C. Peptide separation was carried out using a gradient from 5 to 80% B for 38 min followed by 80% B maintained for 3 min. Then, the column was reconditioned using 5% mobile phase B during 10 min. A volume of 10 μL, corresponding to 2.5 μg of cFEE, was injected and analyzed online with an LTQ-Orbitrap XL mass spectrometer (Thermo-Fisher Scientific, Manchester, U.K.) hyphenated through the intermediate of a heated electrospray ionization probe (HESI-II, Thermo-Fisher Scientific). Data acquisition was controlled by Xcalibur software (Thermo-Fisher Scientific). ESI source parameters were set as follows: ESI voltage of −4.0 kV while sheath gas and auxiliary gas flowrates were set to 40 and 12, respectively. The source heating temperature was set to 300 °C, capillary temperature was set to 320 °C, and capillary voltage to a value of 35 V. The tube lens voltage was set to 90 V. MS/MS was realized in an m/z targeting approach. Fragmentation was performed using collision-induced dissociation (CID). The parameters were set to a normalized collision energy of 35%, an activation time of 30 ms, and an isolation width of 2 Th. The mass/charge (m/z) range was 150−2000 in MS and 100−2000 in MS/MS. Using those parameters, the mean resolution provided by the instrument was 30,000 in MS (m/z = 715.2062).

Spectroscopic Setups and Post-Record Data Analysis. Room-temperature UV-CD spectra were analyzed on a JASCO J-810 spectrophotometer (Lisses, France) within the 190−300 nm spectral range. A path length of 1 mm and a spectral resolution of 0.2 nm were selected. Each spectrum corresponding to an average of five scans was recorded with a speed of 100 nm/min. To facilitate the comparison of the CD spectra recorded in different conditions, the measured ellipticity for each sample, referred to as $[\phi]_{obs}$, was further normalized to obtain the so-called mean residue ellipticity, $[\phi]$, by using the expression: $[\Phi] = \frac{[\Phi]_{obs}}{ncl}$, where n, c, and l are the numbers of residues in the peptide, the molar concentration, and the optical path length of the sample, respectively.[23] The normalized ellipticity was expressed in deg cm^2 $dmol^{-1}$.

Room-temperature Stokes Raman spectra were analyzed at the right angle on a Jobin-Yvon T64000 spectrometer (Longjumeau, France) at a single spectrograph configuration, with a 1200 grooves/mm holographic grating and a holo-

DOI: 10.1021/acsomega.9b01885
ACS Omega 2019, 4, 18049−18060

graphic notch filter. Raman data corresponding to a 1200 s acquisition time for each spectrum were collected on a liquid nitrogen-cooled CCD detection system (Spectrum One, Jobin-Yvon). The effective slit width was set to 5 cm^{-1}. Solution samples were excited by the 488 nm line of an Ar^+ laser (Spectra Physics, Evry, France), with 200 mW power at the sample. Buffer subtraction of the observed spectra was performed using the GRAMS/AI Z.00 package (Thermo Galactic, Waltham, MA, USA). Final presentation of Raman spectra was done by means of the SigmaPlot package 6.10 (SPSS Inc., Chicago, IL, USA).

Quantum Mechanical Calculations. Energetic, geometrical, and vibrational data of cFEE and its building blocks were estimated by the density functional theory (DFT) approach,[53] using the hybrid B3LYP functional.[54,55] Taking into account the structural complexity of the hexapeptide (86 atomic centers), a cost effective, reasonable size Gaussian-type atomic basis set, that is, polarized double zeta enriched with d orbital functions on C, N, and O atoms, referred to as 6-31G(d), was used. Two starting conformers of cFEE (see Results and Discussion for details) were placed in a polarizable continuum model (PCM),[56,57] mimicking methanol (ε_r = 32.63). In contrast, the geometry optimization on free zwitterionic AAs was performed in a solvent continuum with ε_r = 78.39 (corresponding to water) by means of a more extended (triple zeta) basis set additionally equipped with diffuse functions on all atoms, as well as p orbitals on H atoms, referred to as 6-311++G(d,p). Geometry optimization was followed by the harmonic vibration calculation. The absence of any imaginary frequency proved the correspondence of the optimized conformer to a local minimum in the molecular energy landscape. The energy order of the optimized geometries of a given molecular species was determined on the basis of their total energy (E_{tot}), where $E_{tot} = E_e$ + free energy correction. Each optimized conformer was identified by its relative energy (ΔE), that is, its energy difference with that corresponding to the lowest energy one for which $\Delta E = 0$. All quantum mechanical calculations were made using the Gaussian09 package.[58]

■ ASSOCIATED CONTENT

Supporting Information

The Supporting Information is available free of charge on the ACS Publications website at DOI: 10.1021/acsomega.9b01885.

Amino acid composition of the cyclic hexapeptide cFEE, residues are numbered from N^{ter} to C^{ter}, the cyclic structure is maintained by the Cys^1-Cys^6 disulfide linkage (Scheme 1); example of mass spectrum obtained from LC-MS/MS analysis corresponding to the cFEE cyclic peptide (retention time, 10.18 min; theoretical m/z = 715.2062) (Figure S1A); raw MS/MS spectrum corresponding to the fragmentation of the cyclic peptide cFEE (precursor ion, 715.20; charge state, 1+) (Figure S1B); observed and calculated modes of glutamate (Table S1); atomic Cartesian coordinates of cFEE as geometry optimized at the B3LYP/6-31G(d) level in a polarizable continuum mimicking methanol (ε_r = 32.63) (Table S2) (PDF)

■ AUTHOR INFORMATION

Corresponding Author

*E-mail: mahmoud.ghomi@univ-paris13.fr.

ORCID

Belén Henández: 0000-0003-3357-2382
Santiago Sanchez-Cortes: 0000-0002-1081-4644
Sergei G. Kruglik: 0000-0002-2945-3092
Mahmoud Ghomi: 0000-0003-4434-1491

Notes

The authors declare no competing financial interest.

■ ACKNOWLEDGMENTS

The theoretical calculations described here were granted access to the HPC resources of CINES/IDRIS under the allocations A0030805065 (in 2018) and A0060805065 (in 2019) made by Grand Equipement National de Calcul Intensif (GENCI). This work was supported by Spanish Ministerio de Economía, Industria y Competitividad (projects FIS2014-52212-R and FIS2017-84318-R).

■ REFERENCES

(1) Wolfsberg, T. G.; Straight, P. D.; Gerena, R. L.; Huovila, A. P. J.; Primakoff, P.; Myles, D. G.; White, J. M. ADAM, a widely distributed and developmentally regulated gene family encoding membrane proteins with A Disintegrin And Metalloprotease Domain. *Dev. Biol.* **1995**, *169*, 378−383.

(2) Primakoff, P.; Hyatt, H.; Tredick-Kline, J. Identification and purification of a sperm surface protein with a potential role in sperm-egg membrane fusion. *J. Cell Biol.* **1987**, *104*, 141−149.

(3) Almeida, E. A.; Huovila, A. P.; Sutherland, A. E.; Stephens, L. E.; Calarco, P. G.; Shaw, L. M.; Mercurio, A. M.; Sonnenberg, A.; Primakoff, P.; Myles, D. G.; White, J. M. Mouse egg integrin α 6 β 1 functions as a sperm receptor. *Cell* **1995**, *81*, 1095−1104.

(4) Bigler, D.; Takahashi, Y.; Chen, M. S.; Almeida, E. A. C.; Osbourne, L.; White, J. M. Sequence-specific interaction between the disintegrin domain of mouse ADAM 2 (Fertilin β) and murine Eggs. *J. Biol. Chem.* **2000**, *275*, 11576−11584.

(5) Yuan, R.; Primakoff, P.; Myles, D. G. A role for the disintegrin domain of cyritestin, a sperm surface protein belonging to the ADAM family, in mouse sperm-egg plasma membrane adhesion and fusion. *J. Cell Biol.* **1997**, *137*, 105−112.

(6) Pyluck, A.; Yuan, R.; Galligan, E.; Primakoff, P.; Myles, D. G.; Sampson, N. S. ECD peptides inhibit in vitro fertilization in mice. *Bioorg. Med. Chem. Lett.* **1997**, *7*, 1053−1058.

(7) Zhu, X.; Bansal, N. P.; Evans, J. P. Identification of key functional amino acids of the mouse fertilin β (ADAM2) disintegrin loop for cell-cell adhesion during fertilization. *J. Biol. Chem.* **2000**, *275*, 7677−7683.

(8) Fujihara, Y.; Miyata, H.; Ikawa, M. Factors controlling sperm migration through the oviduct revealed by gene-modified mouse models. *Exp. Anim.* **2018**, *67*, 91−104.

(9) Cho, C. Fertilization defects in sperm from mice lacking Fertilin β. *Science* **1998**, *281*, 1857−1859.

(10) Kim, E.; Yamashita, M.; Nakanishi, T.; Park, K. E.; Kimura, M.; Kashiwabara, S.; Baba, T. Mouse sperm lacking ADAM1b/ADAM2 fertilin can fuse with the egg plasma membrane and effect fertilization. *J. Biol. Chem.* **2006**, *281*, 5634−5639.

(11) Ikawa, M.; Inoue, N.; Benham, A. M.; Okabe, M. Fertilization: a sperm's journey to and interaction with the oocyte. *J. Clin. Invest.* **2010**, *120*, 984−94.

(12) Gupta, S. K.; Alves, K.; Palladino, L. O. N.; Mark, G. E.; Hollis, G. F. Molecular cloning of the human fertilin β subunit. *Biochem. Biophys. Res. Commun.* **1996**, *224*, 318−326.

(13) Ziyyat, A.; Naud-Barriant, N.; Barraud-Lange, V.; Chevalier, F.; Kulski, O.; Lemkecher, T.; Bomsel, M.; Wolf, J. P. Cyclic FEE peptide

DOI: 10.1021/acsomega.9b01885
ACS Omega 2019, 4, 18049−18060

increases human gamete fusion and potentiates its RGD-induced inhibition. *Hum. Reprod.* **2005**, *20*, 3452−3458.
(14) Barraud-Lange, V.; Naud-Barriant, N.; Ducot, B.; Chambris, S.; Bomsel, M.; Wolf, J. P.; Ziyyat, A. Cyclic QDE peptide increases fertilization rates and provides healthy pups in mouse. *Fertil. Steril* **2009**, *91*, 2110−2115.
(15) Awasthi, S. K.; Shankaramma, S. C.; Raghothama, S.; Balaram, P. Solvent-induced?-hairpin to helix conformational transition in a designed peptide. *Biopolymers* **2001**, *58*, 465−476.
(16) Hernández, B.; Boukhalfa-Heniche, F. Z.; Seksek, O.; Coïc, Y. M.; Ghomi, M. Secondary conformation of short lysine- and leucine-rich peptides assessed by optical spectroscopies: Effect of chain length, concentration, solvent, and time. *Biopolymers* **2006**, *81*, 8−19.
(17) Guiffo-Soh, G.; Hernández, B.; Coïc, Y. M.; Boukhalfa-Heniche, F. Z.; Ghomi, M. Vibrational analysis of amino acids and short peptides in hydrated media. II. Role of KLLL repeats to induce helical conformations in minimalist LK-peptides. *J. Phys. Chem. B* **2007**, *111*, 12563−12572.
(18) Guiffo-Soh, G.; Hernández, B.; Coïc, Y. M.; Boukhalfa-Heniche, F. Z.; Fadda, G.; Ghomi, M. Vibrational analysis of amino acids and short peptides in hydrated media. 3. Successive KL repeats induce highly stable beta-strands capable of forming non-H-bonded aggregates. *J. Phys. Chem. B* **2008**, *112*, 1282−1289.
(19) Hernández, B.; Carelli, C.; Coïc, Y. M.; De Coninck, J.; Ghomi, M. Vibrational analysis of amino acids and short peptides in aqueous media. V. The effect of the disulfide bridge on the structural features of the peptide hormone somatostatin-14. *J. Phys. Chem. B* **2009**, *113*, 12796−12803.
(20) Hernández, B.; Coïc, Y. M.; Kruglik, S. G.; Carelli, C.; Cohen, R.; Ghomi, M. Octreotide used for probing the type-II′ β-turn CD and Raman markers. *J. Phys. Chem. B* **2012**, *116*, 9337−9345.
(21) Hernández, B.; Coïc, Y. M.; Baron, B.; Kruglik, S. G.; Pflüger, F.; Cohen, R.; Carelli, C.; Ghomi, M. Low concentration structural dynamics of lanreotide and somatostatin-14. *Biopolymers* **2014**, *101*, 1019−1028.
(22) Hernández, B.; Coïc, Y. M.; López-Tobar, E.; Sanchez-Cortes, S.; Baron, B.; Pflüger, F.; Kruglik, S. G.; Cohen, R.; Ghomi, M. Dynamical behavior of somatostatin-14 and its cyclic analogues as analyzed in bulk and on plasmonic silver nanoparticles. *Adv. Protein Chem. Struct. Biol.* **2018**, *112*, 81−121.
(23) Lazo, N. D.; Downing, D. T. Effects of Na2SO4 on hydrophobic and electrostatic interactions between amphipathic alpha-helices. *J. Pept. Res.* **2001**, *58*, 457−463.
(24) Rotival, R.; Bernard, M.; Henriet, T.; Fourgeaud, M.; Fabreguettes, J. R.; Surget, E.; Guyon, F.; Do, B. Comprehensive determination of the cyclic FEE peptide chemical stability in solution. *J. Pharm. Biomed. Anal.* **2014**, *89*, 50−55.
(25) Perczel, A.; Fasman, G. D. Quantitative analysis of cyclic beta-turn models. *Protein Sci.* **1992**, *1*, 378−395.
(26) Kelly, S. M.; Price, N. C. The use of circular dichroism in the investigation of protein structure and function. *Curr. Protein Pept. Sci.* **2000**, *1*, 349−384.
(27) Gibbs, A. C.; Bjorndahl, T. C.; Hodges, R. S.; Wishart, D. S. Probing the structural determinants of type II′ β-turn formation in peptides and Proteins. *J. Am. Chem. Soc.* **2002**, *124*, 1203−1213.
(28) Hernández, B.; Pflüger, F.; López-Tobar, E.; Kruglik, S. G.; Garcia-Ramos, J. V.; Sanchez-Cortes, S.; Ghomi, M. Disulfide linkage Raman markers: a reconsideration attempt. *J. Raman Spectrosc.* **2014**, *45*, 657−664.
(29) Hernández, B.; Pfluger, F.; Adenier, A.; Kruglik, S. G.; Ghomi, M. Vibrational analysis of amino acids and short peptides in hydrated media. VIII. Amino acids with aromatic side chains: L-phenylalanine, L-tyrosine, and L-tryptophan. *J. Phys. Chem. B* **2010**, *114*, 15319−15330.
(30) Hernández, B.; Pflüger, F.; Kruglik, S. G.; Ghomi, M. Characteristic Raman lines of phenylalanine analyzed by a multi-conformational approach. *J. Raman Spectrosc.* **2013**, *44*, 827−833.
(31) Hernández, B.; Pflüger, F.; Adenier, A.; Nsangou, M.; Kruglik, S. G.; Ghomi, M. Energy maps, side chain conformational flexibility, and vibrational features of polar amino acids L-serine and L-threonine in aqueous environment. *J. Chem. Phys.* **2011**, *135*, No. 055101.
(32) Sibanda, B. L.; Thornton, J. M. β-Hairpin families in globular proteins. *Nature* **1985**, *316*, 170−174.
(33) Das, C.; Naganagowda, G. A.; Karle, I. L.; Balaram, P. Designed β-hairpin peptides with defined tight turn stereochemistry. *Biopolymers* **2001**, *58*, 335−346.
(34) Pohl, E.; Heine, A.; Sheldrick, G. M.; Dauter, Z.; Wilson, K. S.; Kallen, J.; Huber, W.; Pfäffli, P. J. Structure of octreotide, a somatostatin analogue. *Acta Crystallogr., Sect. D: Biol. Crystallogr.* **1995**, *51*, 48−59.
(35) Melacini, G.; Zhu, Q.; Goodman, M. Multiconformational NMR analysis of sandostatin (octreotide): equilibrium between beta-sheet and partially helical structures. *Biochemistry* **1997**, *36*, 1233−1241.
(36) Hernández, B.; Lopez-Tobar, E.; Sanchez-Cortes, S.; Coic, Y. M.; Baron, B.; Chenal, A.; Kruglik, S. G.; Pfluger, F.; Cohen, R.; Ghomi, M. From bulk to plasmonic nanoparticle surfaces: the behavior of two potent therapeutic peptides, octreotide and pasireotide. *Phys. Chem. Chem. Phys.* **2016**, *18*, 24437−24450.
(37) Hernández, B.; Pflüger, F.; Dauchez, M.; Ghomi, M. Privileged hydration sites in aromatic side chains: effect on conformational equilibrium. *Phys. Chem. Chem. Phys.* **2017**, *19*, 28684−28695.
(38) Schmidt, B.; Ho, L.; Hogg, P. J. Allosteric disulfide bonds. *Biochemistry* **2006**, *45*, 7429−7433.
(39) Schmidt, B.; Hogg, P. J. Search for allosteric disulfide bonds in NMR structures. *BMC Struct. Biol.* **2007**, *7*, 49.
(40) Cook, K. M.; Hogg, P. J. Post-translational control of protein function by disulfide bond cleavage. *Antioxid. Redox Signaling* **2013**, *18*, 1987−2015.
(41) Hogg, P. J. Targeting allosteric disulphide bonds in cancer. *Nat. Rev. Cancer* **2013**, *13*, 425−431.
(42) Ananthanarayanan, V. S.; Brimble, K. S. Interaction of oxytocin with Ca^{2+}: I. CD and fluorescence spectral characterization and comparison with vasopressin. *Biopolymers* **1996**, *40*, 433−443.
(43) Fric, I.; Hlavacek, J.; Rockway, T. W.; Chan, W. Y.; Hruby, V. J. Effects of conformational constraint in 2- and 8-cycloleucine analogues of oxytocin and [1-penicillamine] oxytocin examined by circular dichroism and biosassay. *J. Protein Chem.* **1990**, *9*, 9−15.
(44) Grzonka, Z.; Gwizdała, E.; Kasprzykowski, F.; ŁaneKiewicz, L. Circular dichroism studies of some arginine-vasopressin analogues. *Biophys. Chem.* **1988**, *31*, 87−100.
(45) Pazderková, M.; Bednárová, L.; Dlouhá, H.; Flegel, M.; Lebl, M.; Hlaváček, J.; Setnička, V.; Urbanová, M.; Hynie, S.; Klenerová, V.; Baumruk, V.; Maloň, P. Electronic and vibrational optical activity of several peptides related to neurohypophyseal hormones: Disulfide group conformation. *Biopolymers* **2012**, *97*, 923−932.
(46) Vale, W.; Grant, G.; Amoss, M.; Blackwell, R.; Guillemin, R. Culture of enzymatically dispersed anterior pituitary cells: functional validation of a method. *Endocrinology* **1972**, *91*, 562−72.
(47) Hallenga, K.; Van Binst, G.; Knappenberg, M.; Brison, J.; Michel, A.; Dirkx, J. The conformational properties of some fragments of the peptide hormone somatostatin. *Biochim. Biophys. Acta, Protein Struct.* **1979**, *577*, 82−101.
(48) Hallenga, K.; Van Binst, G.; Scarso, A.; Michel, A.; Knappenberg, M.; Dremier, C.; Brison, J.; Dirkx, J. The conformational properties of the peptide hormone somatostatin (III). *FEBS Lett.* **1980**, *119*, 47−52.
(49) Knappenberg, M.; Michel, A.; Scarso, A.; Brison, J.; Zanen, J.; Hallenga, K.; Deschrijver, P.; Van Binst, G. The conformational properties of somatostatin IV. The conformers contributing to the conformational equilibrium of somatostatin in aqueous solution as found by semi-empirical energy calculations and high-resolution NMR experiments. *Biochim. Biophys. Acta, Protein Struct. Mol. Enzymol.* **1982**, *700*, 229−246.
(50) Weckbecker, G.; Lewis, I.; Albert, R.; Schmid, H. A.; Hoyer, D.; Bruns, C. Opportunities in somatostatin research: biological, chemical and therapeutic aspects. *Nat. Rev. Drug Discovery* **2003**, *2*, 999−1017.

DOI: 10.1021/acsomega.9b01885
ACS Omega 2019, 4, 18049−18060

(51) Bruns, C.; Lewis, I.; Briner, U.; Meno-Tetang, G.; Weckbecker, G. SOM230: a novel somatostatin peptidomimetic with broad somatotropin release inhibiting factor (SRIF) receptor binding and a unique antisecretory profile. *Eur. J. Endocrinol.* **2002**, *146*, 707−716.
(52) Marshall, G. R. Three-dimensional structure of peptide-protein complexes: implications for recognition. *Curr. Opin. Struct. Biol.* **1992**, *2*, 904−919.
(53) Kohn, W.; Sham, L. J. Self-consistent equations including exchange and correlation effects. *Phys. Rev.* **1965**, *140*, A1133−A1138.
(54) Lee, C.; Yang, W.; Parr, R. G. Development of the Colle-Salvetti correlation-energy formula into a functional of the electron density. *Phys. Rev. B* **1988**, *37*, 785−789.
(55) Becke, A. D. Density-functional thermochemistry. III. The role of exact exchange. *J. Chem. Phy.* **1993**, *98*, 5648−5652.
(56) Barone, V.; Cossi, M. Quantum Calculation of Molecular Energies and Energy Gradients in Solution by a Conductor Solvent Model. *J. Phys. Chem. A* **1998**, *102*, 1995−2001.
(57) Cossi, M.; Rega, N.; Scalmani, G.; Barone, V. Energies, structures, and electronic properties of molecules in solution with the C-PCM solvation model. *J. Comput. Chem.* **2003**, *24*, 669−681.
(58) Frisch, M. J.; Trucks, G. W.; Schlegel, H. B.; Scuseria, G. E.; Robb, M. A.; Cheeseman, J. R.; Scalmani, G.; Barone, V.; Petersson, G. A.; Nakatsuji, H.; Li, X.; Caricato, M.; Marenich, A. V.; Bloino, J.; Janesko, B. G.; Gomperts, R.; Mennucci, B.; Hratchian, H. P.; Ortiz, J. V.; Izmaylov, A. F.; Sonnenberg, J. L.; Williams; Ding, F.; Lipparini, F.; Egidi, F.; Goings, J.; Peng, B.; Petrone, A.; Henderson, T.; Ranasinghe, D.; Zakrzewski, V. G.; Gao, J.; Rega, N.; Zheng, G.; Liang, W.; Hada, M.; Ehara, M.; Toyota, K.; Fukuda, R.; Hasegawa, J.; Ishida, M.; Nakajima, T.; Honda, Y.; Kitao, O.; Nakai, H.; Vreven, T.; Throssell, K.; Montgomery, J. A., Jr.; Peralta, J. E.; Ogliaro, F.; Bearpark, M. J.; Heyd, J. J.; Brothers, E. N.; Kudin, K. N.; Staroverov, V. N.; Keith, T. A.; Kobayashi, R.; Normand, J.; Raghavachari, K.; Rendell, A. P.; Burant, J. C.; Iyengar, S. S.; Tomasi, J.; Cossi, M.; Millam, J. M.; Klene, M.; Adamo, C.; Cammi, R.; Ochterski, J. W.; Martin, R. L.; Morokuma, K.; Farkas, O.; Foresman, J. B.; Fox, D. J. *Gaussian 16* Rev. B.01; Gaussian Inc.: Wallingford, CT, 2016.

DOI: 10.1021/acsomega.9b01885
ACS Omega 2019, 4, 18049−18060